Temporal Evolution of Phase Morphology of Polypropylene/Poly(ethylene octene) Elastomer Binary Polymer Blends by Phase Contrast Microscope

Xinhua Xu, Tianbing Zhu, Xueliang Yan, Chunhuai Zhang

School of Material Science and Engineering, Tianjin University, Tianjin 300072, China

Received 16 March 2006; accepted 13 October 2006
DOI 10.1002/app.25648
Published online 27 February 2007 in Wiley InterScience (www.interscience.wiley.com).

ABSTRACT: Blend films of polypropylene/poly(ethylene-octane) at various mixing times are prepared by freezing-microtome. The temporal evolution of their phase morphologies is investigated by phase contrast microscope (PCM). The digital image analysis, which contains the analysis in both real and wave-number space, is introduced to deal with the PCM graphs. The characteristic length, L in real space, the average domain spacing, and the average chord lengths in wave-number space, are used to express the domain sizes of two phases. The temporal evolution of phase morphology reaches the dynamic equilibrium between breakup and coalescences of domains at the late stage of mixing. In addition, two different fractal dimensions are defined to discuss the symmetry of the distribution of dispersed phase domains and the distribution uniformity: D_f for the symmetry and D_c for the uniformity. © 2007 Wiley Periodicals, Inc. J Appl Polym Sci 104: 2778–2784, 2007

Key words: polypropylene; polyolefins; microstructure; morphology; fractal dimension

INTRODUCTION

The toughening of polymers has been studied for more than half a century. More and more researchers have been focusing on polymer blends. Phase structure of polymer blends during the mixing, which influences their mechanical properties, has attracted much more attention. To obtain materials with pre-eminent performance, many smart people have studied the evolution of the phase morphology during melting and mixing. To control the blend properties, the morphology development during processing should be understood. In general, composition, viscosity ratio, molar mass, elasticity ratio, interfacial tension, shear rate/shear stress, and mixing time play a critical role in the development of microstructure in polymer blends.[1–8] To monitor the phase formation and evolution in time, some smart researchers have studied changes of the phase morphology during the mixing and found that the changes of phase morphology occur within the first 2 min.[8–13]

During the mixing, the phase dimension size decreases promptly at the initial stage. Here, the breakup of domains is preferential because of the shear effect. At the late stage, with the increase of coalescence produced by collision of the dispersed phase domains, the average size of these domains levels off. And the breakup and coalescences of these domains reach a dynamic equilibrium at the last stage.

PP is widely used in packing, textiles, and household goods, but the usefulness of PP is still limited for its poor impact resistance. Therefore, toughening of PP has been a long-standing interest of polymer researchers.[14,15] In recent years, due to the excellent performances of POE with high elasticity, strength, and elongation rate, which is polymerized using metallocene initiator by Dow Chemical Company (Midland, MI), much work has paid more attention to toughening PP, using POE. Many researchers have done much work on mechanical, thermal, rheological, morphological, and interfacial properties of polypropylene/poly(ethylene-octane) (PP/POE) blends.[5,16–21] However, less work is paid attention to dispersion dynamics of the dispersed phase by patterns analysis.

Quantitative description of the phase morphology is rather difficult and there is rarely useful tool to resolve it.[22] Yet, fractal theory is an exciting tool to describe the irregular patterns of the micrographs. Although the fractal theory is very efficient to the micrographs, which have self-similarity, few papers are focused on the applications of the fractal theory in polymer blends. In addition, for polymer blends, micrographs of the phase morphologies represent the spatial distribution and temporal evolution of

Correspondence to: X. Xu (xhxu@tju.edu.cn).
Contract grant sponsor: National Natural Science Foundation of China; contract grant number: 02490220.

such parameters as the concentration and the orientation of the dispersed phase domains, and also, correspond to the phase formation and evolution of polymer blends. As it is known, it is an effective method to use the digital image analysis (DIA) for dealing with micrographs of the phase morphology.[23–27] Using the DIA, not only various information, e.g., dimension and shape of domains of the dispersed phase, but also a power spectrum image obtained by two-dimensional Fourier transformation (2DFT) of the original image can be obtained.

Therefore, in this article, DIA technology and the fractal theory are used to analyze micrographs of PP/POE binary blends, which are obtained by phase contrast microscope (PCM) for finding some useful information about the temporal evolution of phase morphology.

THEORY

Determination of the domain sizes

Characteristic length in real space

A characteristic length of domains, L, is defined as a similar manner with definition given by Guinier and Fournet.[28] L is defined as a span from one side of domains to another, which is shown in Figure 1, and one could easily understand its meaning in real space. To scan the image using a set of lines circling around the centroids of domains for every 2 degrees, a set of L could be easily obtained. And also, average characteristic length, L_m, could be attained by counting L. Using the graph-estimation method,[29] the distribution of L can be studied in detail. If a given t is a positive random variable in $\ln t - N(\mu, \sigma^2)$, t obeys a log-normal distribution and can be expressed as $t - \ln(\mu, \sigma^2)$. Here, μ is the expectation and σ is the standard variance. σ denotes the distribution range of t. The larger σ is, the wider the distribution range is. Therefore, it is appropriate to judge whether the distribution of L obeys a log-normal distribution. Generally, the function of the log-normal distribution is described by

$$F(t) = \frac{\log e}{\sqrt{2\pi}\sigma t}\int_{-\infty}^{t} \exp\left[-\frac{1}{2}\left(\frac{\log t - \mu}{\sigma}\right)^2\right]dt, \quad t > 0 \tag{1}$$

However, this relation is a continuously increasing curve rather than a straight line. It can be expressed by a standard normal distribution function as follows:

$$F(t) = \int_{-\infty}^{\log t - \mu/\sigma} \frac{1}{\sqrt{2\pi}} e^{-x^2/2}dx = \Phi\left(\frac{\log t - \mu}{\sigma}\right), \quad t > 0 \tag{2}$$

Because the standard normal distribution function is a monotonously increasing function, its inverse function exists, expressed by

$$\Phi^{-1}[F(t)] = \frac{\log t - \mu}{\sigma} \tag{3}$$

So if $\Phi^{-1}[F(t)]$ is marked as Y and $\log t$ as X, eq. (3) can be changed to

$$Y = \frac{1}{\sigma}X - \frac{\mu}{\sigma} \tag{4}$$

Obviously, eq. (4) relates to a straight line in the X–Y-frame whose slope is $1/\sigma$ and intercept is $-\mu/\sigma$. Hence, it is found that the log-normal distribution function can be described as an increasing straight line, which was called the graph-estimation method.

Average chord length, average domain spacing in wave-number (h) space

Domain Sizes of dispersed phase in polymer blends can not only be defined in the real space, but also in the wave-number (h) space. For phase contrast micrographs, the images in the h space can be gained by applying 2DFT to the micrographs in the real space. Furthermore, there exists a corresponding relationship between the 2DFT images of micrographs and small-angle light scattering (SALS) images.[30] Therefore, SALS can be used to study the 2DFT images information about phase morphology of polymer blends.

As shown in the Figure 1, one can easily calculate the sizes of the domains using a correlation function. So the authors apply a modification, which fits in spherically symmetrical systems, to Debye–

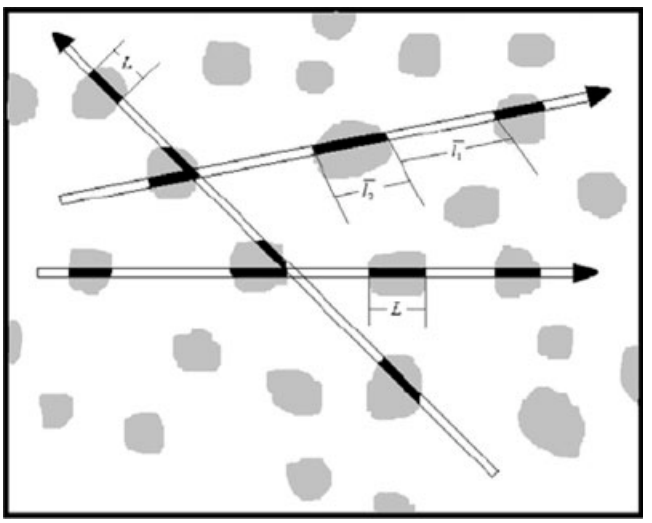

Figure 1 Schematic representation of scanning on a pattern of phase structure and the average chord lengths.

Bueche[31,32] description of scattering from random heterogeneous media,

$$I(h) = K\langle \eta^2 \rangle_{av} \int_0^\infty \gamma(r) \frac{\sin hr}{hr} r^2 dr \quad (5)$$

where K is a proportionality constant and $h = (4\pi/\lambda)\sin\theta$. $\gamma(r)$ is the correlation function. For systems not having a apparently defined structure, $\gamma(r)$ often decreases monotonically with r and may be described by an empirical equation

$$\gamma(r) = \exp(-r/a_c) \quad (6)$$

where α_c is considered as a correlation distance and r defines the size of the heterogeneity. For dilute discrete domains, α_c corresponds to the domain size, while for more concentrated systems, α_c is not simply related to the size of the structural unit but depends on both interdomain and intradomain distances.

If eq. (6) is substituted into eq. (5), one can obtain upon rearrangement,

$$\frac{1}{[I(h)]^{1/2}} = \frac{1}{(K' a_c{}^3)^{1/2}} (1 + h^2 a_c{}^2) \quad (7)$$

In fact, a plot of $I(h)^{-1/2}$ against h^2 may lead to two straight lines (shown in Fig. 2). For SALS where h is small, the corresponding α_{c1} is due to scattering from large domains. As for SALS, when h tends to ∞, the corresponding α_{c2} is due to scattering from the small domains.

Porod[33,34] defines the average chord lengths $\bar{l}_1$ and $\bar{l}_2$, so one can obtain their values by means of formulas as follows:

$$\bar{l}_1 = a_{c1}/\phi_2 \quad (8)$$

$$\bar{l}_2 = a_{c2}/\phi_1 \quad (9)$$

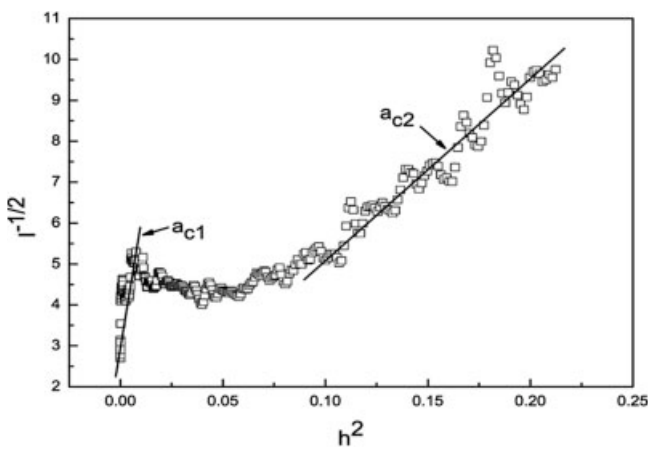

Figure 2 A schematic plot of $I(h)^{-1/2}$ versus h^2.

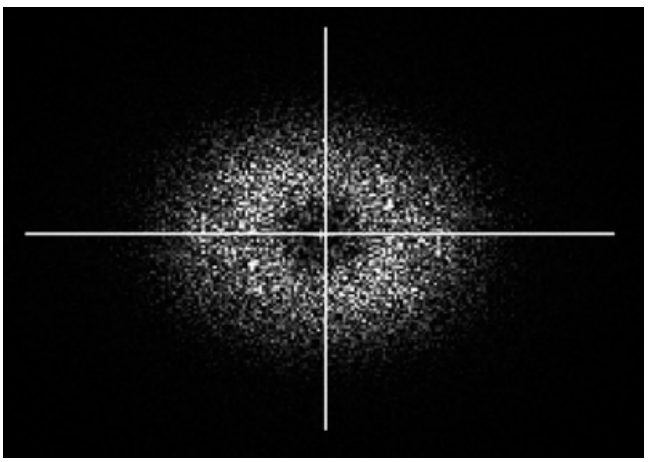

Figure 3 2DFT spectrum with ellipse marked its long axis and short one.

where ϕ_1 is volume fracture of the matrix phase, and ϕ_2 is the volume fracture of the dispersed phase. $\bar{l}_1$ corresponds to the continuous phase, and $\bar{l}_2$ to the dispersed phase, which are shown in Figure 1.

If the 2DFT spectrum is not round but ellipsoidal, the average domain spacing[35] is determined by the average of the minimum and the maximum of interdomain spacings, which are obtained from peak positions of the 2DFT profiles along the white lines shown in Figure 3.

EXPERIMENTAL

Materials

A commercial PP (No.1300, density 0.91 g/cm^3) is supplied by Beijing Yanshan Petrifaction (Beijing, People's Republic of China). POE (No.8150, density 0.868 g/cm^3, ASTM D 792) is obtained from Dow Chemical.

Preparation of blends

The PP and POE are cleaned by distilled water and dried at 40°C in vacuum oven for 5 h. And they are blended in the intermittent mixer (Model XSM-30, mixer with screw diameter 35 mm, made in Shanghai, China). PP and POE elastomer, with the weight ratio of 70/30, are mixed at 200°C at 64 rpm. The blending starts with adding PP and POE into the mixer and the starting point of time is specified as 0 s. The mixing continues for 10 min at 64 rpm. To study the evolution of phase morphology and the dispersion of POE domains in PP matrix, PP/POE blends are obtained, respectively, at 30th s, 1st, 2nd, 4th, 6th, 8th, and 10th min in the blending process. After the acquired blends are taken from the mixer, and then immediately lowed into liquid nitrogen for 10 min, their phase structures can be frozen.

Specimen preparation

The PP/POE blends are cut into specimens for about 30 μm by the freezing-microtome (Leica CM1850, made in Germany). The specimens are observed on a PCM (NIKON Eclipse TE2000-U, made in Japan) with 20 × 10 magnification. Such a thickness makes it possible to neglect the overlapping of domains of the dispersed phase. The micrographs are attained by CCD camera.

RESULTS AND DISCUSSION

Evolution of phase morphology by PCM

According to sequence of the blending time, the micrographs and their corresponding power spectrums, which are obtained by 2DFT of the origin micrographs are shown in the Figure 4. From the 2DFT images, the brightness of the scattering circle becomes increasingly stronger with the blending time.

According to the previously-mentioned theory, the PCM graphs are scanned by a set of different directional lines so that a series of L_m were obtained (shown in Fig. 8). Apparently, before the 4th min, it is the fact that the average characteristic length of the dispersed phase domains decreases gradually, and then levels off. By means of the SALS theory, the average chord length $\bar{l}_2$ of the dispersed phase domains can be calculated (shown in Fig. 5). The trend of $\bar{l}_2$ is consistent with that of L_m during the blending. Therefore, it is appropriate to apply the 2DFT and SALS theory to PCM graphs for calculating the corresponding parameters, which mark the phase morphology. The average chord length of continuous phase, $\bar{l}_1$, grows gradually before the 4th min, and then levels off. At the initial stage of blending, the domain sizes of the POE phase are larger generally and the distances of these domains are shorter apparently because the domains have not still fully been broken up into small droplets under the shearing effect, though they may be soften or melted. At the same time, the domains of POE are not uniform but clustered, so the average distance of these domains is shorter. Although there are collisions and coalescences in these small droplets, they are not of predominance. After the initial stage, with the help of the shearing effect, melted domains have broken up adequately into small ones, the range of whose distribution in the domains size turns to be narrower. The average domain size will decrease, while the average distance of the interdomains increases. In the light of the increase in number of the small domains, the chance of collisions and coalescences is enhanced largely. Therefore, the domains reach a dynamic equilibrium between collisions or coalescences and dispersions. As a result, the average domain size and the average distance of the interdomains reach a steady value. Changes in parameters with the blending time are similar with

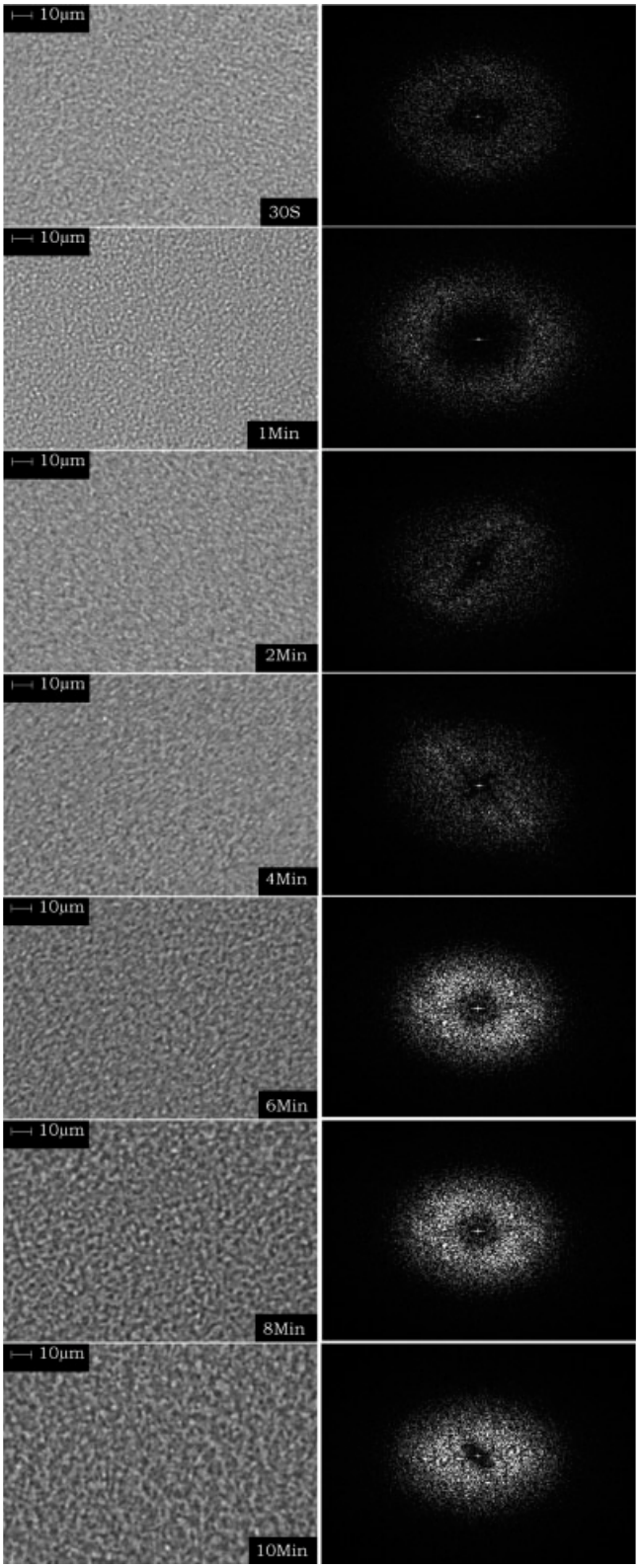

Figure 4 PCM graphs (left) and their corresponding 2DFT images (right) of PP/POE blends.

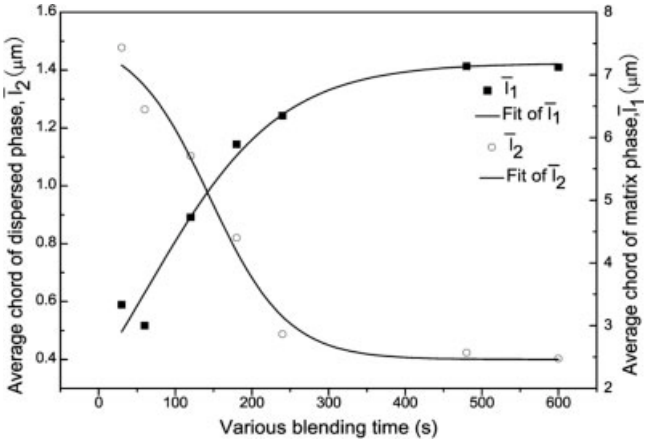

Figure 5 Curves of the average chord length of PP/POE (70/30) blends at different mixing times.

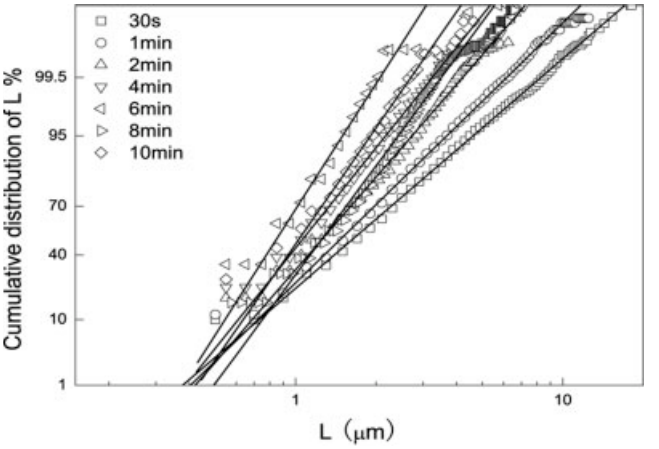

Figure 7 $P[F(L)] - L$ plots of PP/POE (70/30) blends at different mixing times.

those provided in references,[8–13] but a slight difference between the results and the references[8–13] lies in the temporally different starting point at the initial stage of blending. These parameters can represent the temporal evolution of the phase morphology and the dynamics in a way.

In addition, according to the peak position of the 2DFT profile along the white lines shown in Figure 3, the average interdomain spacings of PP/POE (70/30) blends at different mixing times are calculated and showed in Figure 6. From the figure, it is obvious that the average interdomain spacing increases distinctly before the 4th min, and after that, levels off basically. The trend of the average interdomain spacing is similar with $\bar{l}_1$, and it may denote that the average interdomain spacing corresponds to $\bar{l}_1$. Once again, it is reasonable to apply the SALS and the 2DFT theory to PCM graphs for analyzing the morphology of blends.

In Figure 7, the relation between the cumulative distribution of L, that is $P[F(L)]$, and L is shown. The relation between $P[F(L)]$ and L obeys a logarithmic linear one in most range of the domain size. According to the previously mentioned theory, it can be concluded the distribution of L obeys the log-normal distribution. Besides the distribution of L referred earlier, the spatial distribution of the dispersed phase domains, can be deeply explored by a nonlinear mathematical method, the fractal dimension. The relation between number of squares $[N(r)]$ and the fractal dimension obeys a power law on the basis of box-counting method expressed by

$$N(r) \propto r^{-D_f} \tag{10}$$

where r is a kind of length, and D_f is the fractal dimension. However, the fractal dimension is calculated in dimensionless region shown in Figure 8. The authors' cover points in the space with the

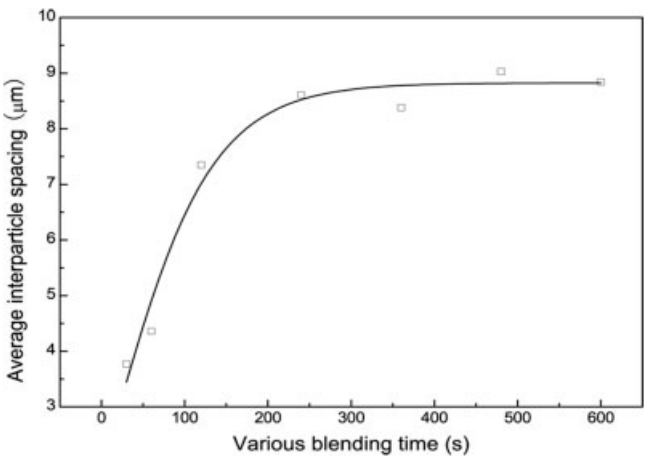

Figure 6 Curve of the average interdomain spacing of PP/POE (70/30) blends at different mixing times.

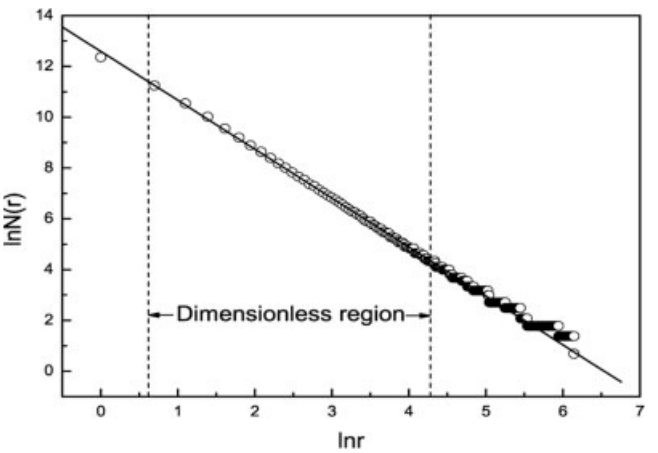

Figure 8 A schematic representation of the dimensionless region.

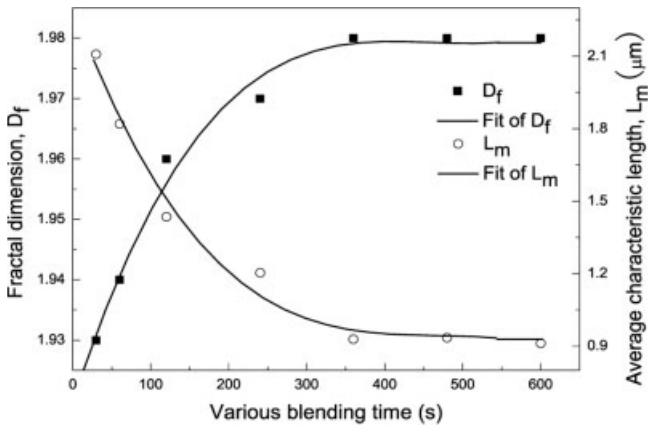

Figure 9 D_f and L_m curves of PP/POE (70/30) blends at different mixing times.

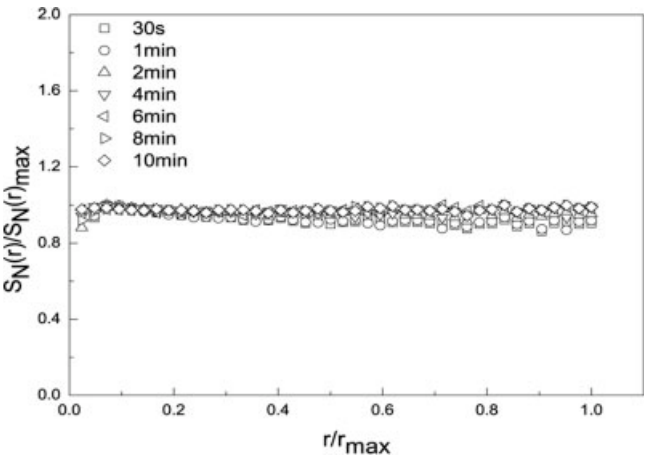

Figure 10 $S_N(r)/S_N(r)_{max} - r/r_{max}$ curves of PP/POE (70/30) blends.

square whose border length is r and note down the number of the squares that at least contain one point by $N(r)$. Thus, the fractal dimension can be obtained by plotting log $N(r)$ against log r. D_f is introduced to describe dispersing state of the dispersed phase domains. Figure 9 shows the D_f values of PP/POE blend at different mixing times at 30% POE fraction.

It is obvious that in the dimensionless region, D_f grows gradually before the 4th min and from then on, levels off as shown in Figure 9. At the start of blending, the dispersed phase domains are not dispersed fully and most of these domains should be large, which can influence on the dispersion. At that time, these domains have not yet taken up the whole two-dimensional plane. Based on the kind of fractal dimension, one can fully consider the dispersion as a fractal structure. After that, with the help of the shearing effect of rotors, the number of the domains becomes more and more, and the domains are dispersed more symmetrically, especially after the 6th min. At last, the fractal dimension grows up to a steady value, that is 1.98, but it doesn't reach 2. It is reasonable to explain the phenomena by the fact that collisions and coalescences of more and more dispersed domains have an influence on the dispersion. Under the shearing effect, both the coalescence and dispersion reach the equilibrium rather than the dispersion of the dispersed phase domains only, so the fractal dimension should range from 1 to 2.

To prove that the phase morphology has self-similarity, it is necessary to introduce a scale function $[S_N(r)]$, which is defined by a formula as follows:

$$S_N(r) = N(r)r^{D_f} \tag{11}$$

Curves of the scale function of PP/POE blends at different mixing times are shown in Figure 10. As shown in Figure 10, the fact that the scale ratios fluctuate on a steady value proves phase morphology to be the fractal character. Besides the fractal structure of the distribution, the authors also introduce the other fractal dimension (D_c) to describe that the distribution is uniform and isotropic by using a correlative density function.

Suppose $\rho(x)$ as the density at a position x of a set of points which are a random distribution in the space. The correlative density function $c(r)$ is given by

$$c(r) = \langle \rho(x)\rho(x+r) \rangle \tag{12}$$

where $<\cdot>$ denotes an average. If the distribution is uniform and isotropic, $c(r)$ is a function which only relates to the distance, r, between two points. Commonly, an exponential function $\exp(r/r_0)$ or a Gaussian function $\exp(-r^2/{r_0}^2)$ is assumed as the correlation function in theoretical model. However, they can't be introduced to the fractal theory because both of them have an r_0. Any couple of points whose distance is less than r_0 are relative with each other, but the correlation decays rapidly when the distance is more than or equal to r_0. On the other hand, if the phase morphology is fractal, the correlative density function obeys a power law. Hence, it is expressed by a relation, in which there is no r_0, given as follows,

$$c(r) \propto r^{-\alpha} \tag{13}$$

And the $C(r)$ becomes $2^{-\alpha}$ times as small as before when the distance of the two points becomes 2 times as long as before. The relation between the exponent α and the fractal dimension D_c can be expressed simply by

$$D_c = d - \alpha \tag{14}$$

where d denotes the spatial dimension.

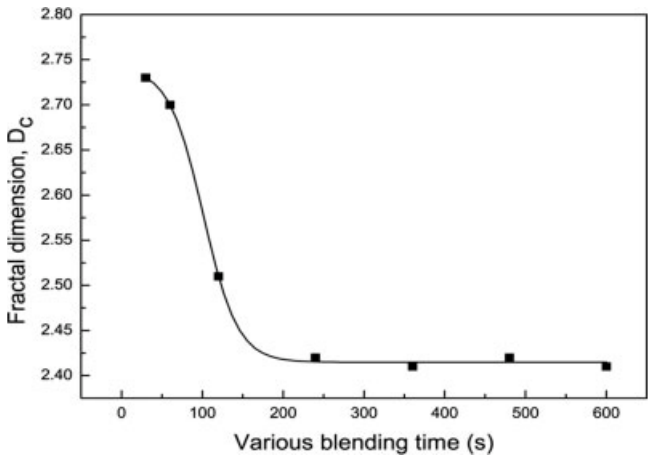

Figure 11 Plot of D_c at different mixing times.

If the correlative density function $c(r)$ scales as eq. (14), its Fourier transform $I(h)$, that is the power spectrum, should also obey a power law. In fact, if $0 < d - D_c < 1$, there is,

$$I(h) = 4\int_0^\infty c(r)\cos(2\pi hr)dr \propto h^{d-D_c-1} \qquad (15)$$

According to the relation, D_c can be estimated easily from the power spectrum. D_c denotes that if the points cluster together, they have an intimate correlation and D_c is larger, which illuminates that the scattering uniform is imperfect.

Figure 11 represents the relation between D_c and the different mixing times. The change in D_c is divided into two stages. Obviously, before the 4th min, D_c decreases so rapidly that the uniformity of the spatial distribution becomes more perfect. From then on, D_c levels off at a smaller value under the dynamic equilibrium of the breakup and coalescence of the dispersed phase domains. Thus, the uniformity is invariable in general.

CONCLUSIONS

The results of the real space show that the distribution of the characteristic length obeys a log-normal one and the initial stage is the main stage of the evolution of phase morphologies. The initial stage is mainly from the very beginning until the 4th min. At this stage, the larger dispersed phase domains may be broken up into smaller ones, and the average size of the domains decreases. At the last stage, the average size levels off at a smaller value. The dispersed phase domains reach the dynamic equilibrium between breakup and coalescences at the late stage of mixing. The results of the wave-number space, obtained by using DIA, which mainly contains 2DFT and SALS theories, accord with those of the real space. It is valid to apply the DIA technology to the PCM graphs.

In addition, in the given scale and range, the spatial distribution of domains of dispersed phase exists a fractal property, and the distribution is closer to two-dimension with the mixing time. Meanwhile, the other fractal dimension decreases rapidly at the initial stage and later on, levels off at a smaller value, which denotes that the uniformity of the distribution becomes more perfect.

References

1. Jelcic, Z.; Holjevac-Grguric, T.; Rek, V. Polym Degrad Stab 2005, 90, 295.
2. Li, Y.; Zhang, Y.; Zhang, Y. X. Polym Test 2004, 23, 83.
3. Puka'nszky, B. Eur Polym J 2005, 41, 645.
4. Sacchi, A.; Landro, D. L.; Pegoraro, M.; Severini, F. Eur Polym J 2004, 40, 1705.
5. McNally, T.; McShane, P.; Nally, M. G.; Murphy, R. W.; Cook, M.; Miller, A. Polymer 2002, 43, 3785.
6. Joseph, S.; Thomas, S. Eur Polym J 2003, 39, 115.
7. Everaerta, V.; Aertsb, L.; Groeninckx, G. Polymer 1999, 40, 6627.
8. Scott, E. C.; Macosko, W. C. Polymer 1995, 36, 461.
9. Shih, C. K. Polym Eng Sci 1995, 35, 1688.
10. Favis, B. D. J Appl Polym Sci 1990, 39, 285.
11. Scott, C. E.; Macosko, C. W. Polym Bull 1991, 26, 341.
12. Sundararaj, U.; Macosko, C. W.; Rolando, R. J.; Chan, H. T. Polym Eng Sci 1992, 32, 1814.
13. Lindt, J. T.; Ghosh, A. K. Polym Eng Sci 1992, 32, 1802.
14. Bucknall, C. B. Adv Polym Sci 1978, 27, 121.
15. Mirabella, O.; Francis, M. J Polym Sci Part B: Polym Phys 1994, 32, 1205.
16. Yang, J. H.; Zhang, Y.; Zhang, Y. X. Polymer 2003, 44, 5047.
17. Da-Silva, N. L. A.; Rocha, G. C. M.; Coutinho, B. M. F.; Bretaf, R.; Scuracchio, C. Polym Test 2000, 19, 363.
18. Da-Silva, N. L. A.; Tavares, B. I. M.; Politano, P. D.; Coutinho, B. M. F.; Rocha, G. C. M. J Appl Polym Sci 2005, 1997, 66.
19. Da-Silva, N. L. A.; Rocha, G. C. M.; Coutinho, B. M. F.; Bretaf, R.; Scuracchio, C. J Appl Polym Sci 2000, 75, 692.
20. Paul, S.; Kale, D. D. J Appl Polym Sci 2002, 84, 665.
21. Godail, L.; Packham, E. D. J Adhes Sci Technol 2001, 15, 1285.
22. Miyata, T.; Takagi, T.; Higuchi, J. I.; Uragami, T. J Polym Sci Part B: Polym Phys 1999, 37, 1545.
23. Fredrickson, G. H.; Binder, K. J Chem Phys 1989, 91, 7265.
24. Takenaka, M.; Hashimoto, T. J Chem Phys 1992, 96, 6177.
25. Hashimoto, T.; Takenaka, M.; Lzumitani, T. J Chem Phys 1992, 97, 679.
26. Alexander, E. R.; Hayashi, M.; Martin, W.; Hashimoto, T. Macromolecules 2000, 33, 2786.
27. Li, Y. Y.; Wang, Y.; Sheng, J. J Macromol Sci Phys 2005, 44, 665.
28. Guinier, A.; Fournet, G. Small Angle Scattering of X-ray; Wiley: New York, 1955.
29. Fang, K. T.; Xu, J. L. Statistics Distribution; China Science Press: Beijing, 1987; pp 136–158.
30. Tanaka, H.; Hayashi, T.; Nishi, T. J Appl Phys 1986, 59, 3627.
31. Debye, P.; Bueche, A. J Appl Phys 1944, 20, 518.
32. Debye, P., Jr.; Anderson, H. R.; Brumberger, H. J Appl Phys 1957, 28, 679.
33. Kratky, O. Pure Appl Chem 1966, 12, 483.
34. Stern, F. Trans Faraday Soc 1955, 51, 430.
35. Alexander, E. R.; Okumura, A.; Matsushige, K.; Hashimoto, T. Macromolecules 2001, 34, 8239.